Assessing the porosity and shrinkage of alkali activated slag-fly ash composites designed applying a packing model

Construction and Building Materials 119 (2016) 175–184

Contents lists available at ScienceDirect

Construction and Building Materials

journal homepage: www.elsevier.com/locate/conbuildmat

Assessing the porosity and shrinkage of alkali activated slag-fly ash composites designed applying a packing model

X. Gao [a,b], Q.L. Yu [a,*], H.J.H. Brouwers [a,b]

[a] Department of the Built Environment, Eindhoven University of Technology, P.O. Box 513, 5600 MB Eindhoven, The Netherlands
[b] State Key Lab of Silicate Materials for Architectures, Wuhan University of Technology, Wuhan 430070, PR China

HIGHLIGHTS

- A particle packing model is used to design alkali activated slag-fly ash composites.
- The relation between porosity and ingredients of alkali activated binder is studied.
- Activator modulus of 1.4 presents the optimum strength in all cases.
- Lowering activator modulus and slag content is efficient to reduce drying shrinkage.

ARTICLE INFO

Article history:
Received 12 February 2016
Received in revised form 2 May 2016
Accepted 5 May 2016

Keywords:
Mix design
Alkali activation
Slag-fly ash blends
Fresh behavior
Porosity
Strength
Drying shrinkage

ABSTRACT

This paper addresses the fresh behaviors, gel structure, strength, porosity and drying shrinkage of alkali activated slag-fly ash composites designed by applying the modified Andreasen & Andersen model. The results show a large variation of slump flows and setting times when using different slag/fly ash ratios and activator moduli. The microstructure analyses by FTIR and TG show the gel structure remains stable after 1 d of curing, and mixes with higher slag contents and lower activator moduli show slightly higher bound water content. The main reaction product is a chain structured C-A-S-H type gel regardless of slag/fly ash ratio and activator modulus, but a slightly higher main absorption band is shown in samples with high fly ash contents. A 28-d compressive strength of about 90 N/mm^2 is achieved and a higher content of slag leads to a higher strength and lower porosity in general. An optimum activator modulus of 1.4 in terms of strength is shown, while an increase of activator modulus between 1.0 and 1.8 benefits the pore structure refinement. Both slag content and activator modulus strongly affect the drying shrinkage, and using a high amount of fly ash and low activator modulus can effectively reduce the drying shrinkage.

1. Introduction

Alkali activated materials (AAM) have been extensively studied in recent years due to their lower environmental impacts [1,2] compared to ordinary Portland cement (OPC) and superior performances such as mechanical properties [3], durability [4], thermal resistance [5] and acid resistance [6]. This type of material is usually produced by mixing alkaline activator solutions with solid precursors. The most commonly used activators are sodium hydroxide, carbonate, silicate or a mixture of those; while the solid raw materials are usually amorphous Ca, Si and Al contained powders such as slag, fly ash, metakaolin, silica fume, red mud and natural pozzolans. Based on the chemical composition of the raw materials, alkali activated materials can be classified into two types: calcium and silica enriched (Ca + Si) system and aluminosilicates dominated (Si + Al) systems [7]. The typical precursor of calcium enriched system is ground granulated blast furnace slag, having a tobermorite-like C-A-S-H gel with a low Ca/Si ratio and a high Al content as major reaction product [8]. The represented materials of Si + Al systems are class F fly ash or metakaolin, having three-dimensional N-A-S-H type gels as the major products [9]. Both systems exhibit distinct behaviors due to their differences in reaction mechanism and gel characteristics.

Recently, growing interests have been paid to blended alkali systems (Na_2O-CaO-Al_2O_3-SiO_2 systems) that are prepared by mixing high calcium contained raw materials with low calcium aluminosilicates, since the blended binder system exhibits modified properties regarding setting times, workability, shrinkage, mechanical properties and durability compared to the individual ones [10–13]. The structure of the reaction products in the blended system is mainly depending on the activator type and dosage, raw

* Corresponding author.
E-mail address: q.yu@bwk.tue.nl (Q.L. Yu).

http://dx.doi.org/10.1016/j.conbuildmat.2016.05.026
0950-0618/

materials composition and curing conditions. Micro-scale investigations identified that the reaction products are generally stably coexisting C-(A)-S-H and N-A-S-H type gels with high amounts of cross-linking [14–16,69]; also the large amount of available calcium and aluminate affect the original structure of N-A-S-H and C-(A)-S-H gels, respectively [17–19]. The recent achievements in understanding the blended alkali systems provide solid theoretical support for the further researches; also those modified properties demonstrate a promising future for the application of alkali activated materials.

On the other hand, it is commonly accepted that an optimal packing of granular ingredients is the key for achieving excellent mechanical strength and durable structures [20–22], and several mix design methods have been proposed in cement based system such as the Linear Packing Density Model, Solid Suspension Model and Compressive Packing Model [23–25]. Among those design methodologies, the modified Andreasen & Andersen particle packing model, which is based on the integral particle size distribution approach of continuously graded mixes [26], shows conveniences by considering fine particles into the design process. While presently, when designing the recipes of alkali activated blended mortars and concretes, key manufacturing parameters from the aspects of activator and raw material are the main concerns, while to the authors' knowledge limited attention has been paid to the packing of the granular ingredients. It is possible that by giving additional consideration to the particle packing in the mix design stage, the binders in alkali activated system will be used in a more efficient manner, while certain fresh and hardened properties may also improve as a result.

Another important issue of alkali activated materials is the shrinkage, since it is well linked to the cracking tendency and consequently the durability related properties. The previous investigations revealed that the alkali activated high calcium system usually exhibits a higher degree of drying shrinkage than the cement based system [27,28], while the alkali low calcium systems can show a lower value than OPC [29]. It was also concluded the activator type and content, the physicochemical properties of the raw material and curing conditions are the key factors that affect the shrinkage behaviors [30,31]. However, there still exists very limited study about the relationships between key synthesizing factors and the shrinkage in alkali activated blended systems. In overall, the objective of this study is to design the room temperature cured alkali activated slag-fly ash blended mortars by applying the modified Andreasen & Andersen particle packing model; while the effects of key synthesizing factors on shrinkage and porosity are investigated. In addition, the fresh behaviors, gel structure development and compressive strength are also addressed and their relations with shrinkage and porosity are discussed.

2. Experiment

2.1. Materials

The solid precursors used in this study were ground granulated blast furnace slag (GGBS, provided by ENCI B.V., the Netherlands) and a commercial Class F fly ash. Their major chemical compositions were analyzed by X-ray fluorescence and are shown in Table 1. Besides, limestone powder was used as filler while a micro sand (0–1 mm, provided by Graniet-Import Benelux B.V., the Netherlands) and a normal sand (0–2 mm) were used as fine aggregates. The specific densities of solid materials are presented in Table 2 while the detailed particle size distributions of all solid materials are given in Fig. 1. Concerning the alkaline activators, a mixture of sodium hydroxide (pellets, analytical level of 99 wt.%) and commercial sodium silicate solution (27.69% SiO_2, 8.39% Na_2O and 63.92% H_2O by mass) was used, due to the advantages in providing additional silicate and continuous alkali conditions of this activator. The desired activator modulus (Ms, SiO_2/Na_2O molar ratio) was achieved by adding the appropriate amount of sodium hydroxide into the sodium silicate solution. Distilled water was added in order to reach the desired water/binder ratio. The mixed activator solution was cooled down to room temperature for 24 h before further use.

Table 1
Major chemical composition of slag and fly ash.

Oxides (wt.%)	FA	GGBS
SiO_2	54.62	34.44
Al_2O_3	24.42	13.31
CaO	4.44	37.42
MgO	1.43	9.89
Fe_2O_3	7.21	0.47
Na_2O	0.73	0.34
K_2O	1.75	0.47
SO_3	0.46	1.23
LOI	2.80	1.65

Table 2
Specific densities of the solid materials.

Solid materials	Specific density (kg/m^3)
Slag	2930
Fly ash	2300
Limestone powder	2710
Micro sand	2720
Normal sand	2640

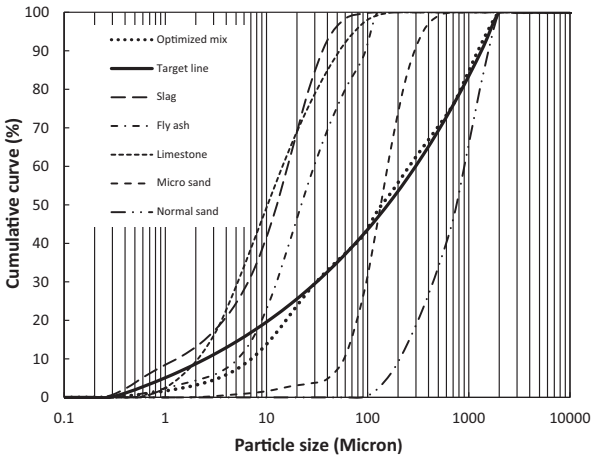

Fig. 1. Particle size distributions of the raw materials, the target curve and the resulting integral grading line of a sample mix.

2.2. Mix design methodology

The mixes of alkali activated slag-fly ash mortars were designed using the modified Andreasen and Andersen (A&A) model in order to maximize the packing of the granular solid materials:

$$P(D) = \frac{D^q - D_{min}^q}{D_{max}^q - D_{min}^q} \quad (1)$$

where P(D) is a fraction of the total solids materials that are smaller than the particle size D (μm), D_{max} is the maximum particle size (μm), D_{min} is the minimum particle size (μm) and q is the distribution modulus. The distribution modulus (q) in the modified A&A model is used to determine the proportion between the fine and coarse particles in the mixture. Higher values of q would lead to a coarse mixture; while lower values will result in mixes with enriched fine particles and result in an increased water demand. Brouwers [32,33] suggested that a theoretically q value range of 0–0.28 would result in an optimal packing. Hunger [21], Yu [65], Ng [67] and Borges [68] recommended a q value in the range of 0.20–0.25 for the design of cement, geopolymers and gypsum as the binder. In order to achieve an ideal workability, the value of q is fixed at 0.23 for all mixtures in this study.

The proportions of each individual material in the mix are adjusted until an optimum fit between the composed mix grading curve and the target curve is reached, using an optimization algorithm based on the least squares method (LSM), namely the deviation between the target curve and the composed mix expressed by the residual sum of squares (RSS) at defined particle sizes is minimal [22,36]. Therefore, the optimized mixture will possess a compact matrix due to the optimal packing. This mix design method has been successfully adopted to design concretes with different types [34,35,65]. An example of the detailed mix designs

Table 3
Mix proportions of alkali-activated slag-fly ash composites (kg/m^3).

Mix	Activator	Slag	Fly ash	Limestone	Sand 0–1	Sand 0–2
M1-820	368.5	463.7	115.9	144.9	271.7	815.1
M2-824	379.8	461.9	115.5	144.3	270.6	811.9
M3-828	390.9	460.1	115.0	143.8	269.6	808.7
M4-640	364.4	343.9	229.3	143.3	268.7	806.1
M5-644	375.6	342.6	228.4	142.7	267.7	802.9
M6-648	386.7	341.3	227.5	142.2	266.6	799.9
M7-460	360.4	226.8	340.2	141.7	265.8	797.3
M8-464	371.5	225.9	338.9	141.2	264.7	794.2
M9-468	382.5	225.1	337.6	140.7	263.7	791.2

based on the modified Andreasen & Andersen particle packing model is shown in Fig. 1, and the detailed mix proportions of the used materials are listed in Table 3. Since there are no suitable superplasticizers in alkali activated system, a relatively low water content is used to optimize the packing while also with the consideration on the flowability. It should be noted that this mix design methodology is based on the volumetric fractions of all used materials, including both solids and liquids. In Portland cement system, the liquid component is primarily water; while in the case of alkali activated system, the liquid (activator) consists of water, dissolved NaOH and sodium silicates. Based on the fact that both NaOH and the silicates in water-glass are well dissolved in the activator solution, their effects on the solids' packing is not taken into account here; while the densities of the liquid activator are calculated based on each individual mix and applied in the packing model.

2.3. Sample preparation

The activators used in this study have an equivalent sodium oxide (Na_2O) content of 5% by mass of the powder and activator moduli of 1.0, 1.4 and 1.8. The target activator modulus was reached by mixing sodium silicate solution and sodium hydroxide pellets with a solution/pellets mass ratio of 3.82, 6.41 and 10.27, respectively. The water/powder ratio was kept constant as 0.4 in all mixtures. The water consisted of the added distilled water and the water contained in the activator solution. Slag/fly ash ratios of 80/20, 60/40 and 40/60 by mass were used. All mortar specimens were prepared in a laboratory mixer; firstly the solid precursors were added into the mixer and mixed for 1 min, followed by the activating solution; the ingredients were mixed at a slow speed for 30 s and rested for 30 s before another 120 s at a medium speed. Then the fine fillers and aggregates were added and another 120 s of mixing was performed. The fresh mortar was then poured into plastic molds of $40 \times 40 \times 160$ mm^3 and vibrated for 1 min, covered with a plastic film on the top surface for 24 h; finally all specimens were demolded and cured at a temperature of 20 °C and a relative humidity of 95% until their testing age.

2.4. Testing methods

The workability of mortar samples were tested by the mini spread-flow test according to EN 1015-3 [37]. Fresh samples were transferred into a standard conical ring and a free flow without jolting was allowed. Two diameters that are perpendicular to each other were determined and the mean value was recorded as the slump flow. The initial and final setting times were measured by a Vicat needle method as described in EN 196-3 [38].

Fourier transform infrared spectroscopy (FTIR) tests were performed in a Varian 3100 instrument with the wavenumbers ranging from 4000 to 600 cm^{-1} at a resolution of 1 cm^{-1}. The thermo-gravimetric (TG) analyze were conducted by using a STA 449 F1 instrument, samples were heated up to 1000 °C at a rate of 5 °C/min with nitrogen as protective gas. The temperature was held isothermally at 105 °C for 1 h during the heating process. Both FTIR and TG analyses were carried out at the age of 1, 7 and 28 d, respectively.

The compressive strength tests were carried out according to EN 196-1 [39]. $40 \times 40 \times 40$ mm^3 cubes were prepared and tested at the ages of 7 and 28 d, and the compressive strength value for each sample was obtained from the average of six specimens.

The porosity was measured by applying the vacuum-saturation technique following the description given in NT Build 492 [40]. The water permeable porosity is calculated as:

$$P(\%) = \frac{Ms - Md}{Ms - Mw} \times 100\% \quad (2)$$

where P (%) is the water permeable porosity, Ms (g) refers to the mass of the saturated sample in surface-dry condition in air, Mw (g) is the mass of water-saturated sample in water and Md (g) is the mass of oven dried sample.

The samples for drying shrinkage test were cast in molds with dimensions of $40 \times 40 \times 160$ mm^3 and cured in sealed condition at a temperature of 20 °C. After 24 h of curing, specimens were exposed in a cabinet with a temperature of 20 °C and relative humidity of 50%, also the initial length (L_0) was measured at that time. Afterwards, the length (L_n) was measured once per day until the age of 28 d. The length change was calculated as:

$$L(\%) = \frac{L_0 - L_n}{L_i} \times 100\% \quad (3)$$

where L_i is the effective initial length.

3. Results and discussion

3.1. Flowability and setting times

The slump flows of the fresh alkali activated slag-fly ash mortars are presented in Fig. 2. The influence of raw materials' composition and activator modulus on the workability is briefly depicted. It can be seen that the activator modulus exhibits a more significant effect on the slump flow than slag/fly ash ratio in general. For instance, in samples with a constant activator modulus of 1.0, the slump flow increases from 16.4 to 18.7 cm when shifting the slag/fly ash ratio from 80/20 to 40/60. Similar results are also shown in mixes with other activator moduli. This can be simply explained by the different water demand between slag and fly ash that is caused by their morphology differences, where slag usually presents a more angular particle shape and larger surface area. On the other hand, compared to the effect of slag/fly ash ratio, a higher range of flowability is shown in samples with a different activator modulus. For a fixed slag/fly ash ratio of 80/20, when increasing the activator modulus from 1.0 to 1.4 and then 1.8, the slump flow is increased from 16.4 cm to 23.6 cm and 26.5 cm; the increase rate is 43.9% and 61.6%, respectively. Dramatic increases in slump flow are also found in samples with other slag/fly ash ratios. One possible explanation for the higher influence of the activator modulus on flowability is that the additional provided silicate from activator benefits the workability due to the nature of the silicate groups, since higher activator modulus means a higher proportion of sodium silicate in the activator solution. In addition, compared to [56], similar flowability is achieved in this study while a lower water to binder ratio is used. It is suggested that more available water can be provided to lubricate the particles by applying the packing model, this is also confirmed by [66]. This is particularly important in the case of alkali activated systems, where no effective superplasticizers are available and limited solution leads to a poor workability [61]. Activator with lower modulus usually exhibits a more intensive reaction at early stages [48], it is also possible that a faster dissolution of the raw materials increases

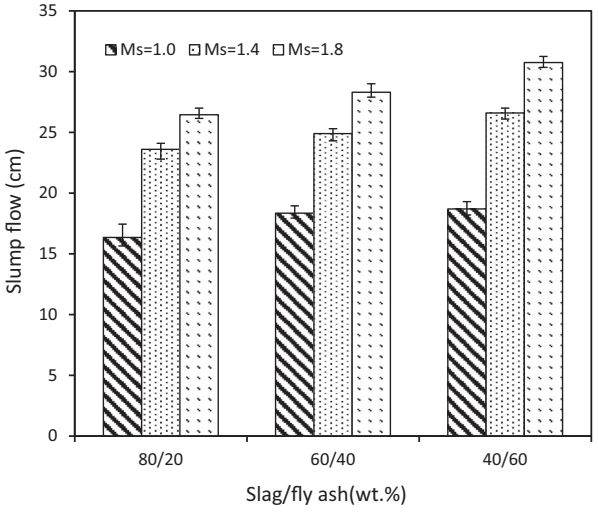

Fig. 2. Slump flow of AA slag-fly ash mortars.

the viscosity of the fresh mortars and results in a reduced slump flow.

Fig. 3 depicts the initial and final setting times of alkali activated slag-fly pastes. It is clear that both slag/fly ash ratio and activator modulus have a significant effect on the setting times; samples with a lower activator modulus and a higher slag content exhibit faster initial and final setting times in general. For instance, when a constant activator modulus of 1.0 is used, the sample with a slag/fly ash ratio of 80/20 shows an initial/final setting time of 10/46 min, whereas 48/84 min in the sample with a slag/fly ash ratio of 40/60. A similar remarkable increment is also observed in samples with other fixed activator moduli when lowering the slag content in the mixture. This can be explained by the higher reactivity of slag than fly ash under ambient temperature. The amorphous structure of slag, with enriched network-modifying cations (primarily Ca), is easier to dissolve than the aluminosilicates dominated structure of fly ash under alkali conditions. Thus as a result of the faster dissolution rate of Ca, Si and Al groups from the precursors, a faster reaction process and a shorter setting time followed. Similar to the effect of the slag/fly ash ratio, dramatic increases of setting times are shown when the activator modulus is increased. As can be seen in Fig. 3, for a constant slag/fly ash ratio of 60/40, the initial/final setting time increases from 29/69 min to 60/110 min when shifting the activator modulus from 1.0 to 1.8, the increasing rate is 107% and 59.4% for the initial and final setting time, respectively. The corresponding increasing rate in samples with a slag/fly ash ratio of 40/60 is 73.9% and 59.3%, respectively. Such significant changes in the setting times indicate that the activator modulus may strongly affect the early age reaction kinetics. In overall, both of the discussed manufacturing factors strongly affect the fresh behaviors of alkali activated slag-fly ash blends; and a large variation in slump flow and setting time can be caused. Thus when designing the mix proportions of this type of material, attention should be firstly paid to the effect of the key synthesizing factors on the fresh behavior.

3.2. FTIR analysis

The infrared spectra of the unreacted slag and fly ash are given in Fig. 4. It is clear that the original slag shows a main vibration band that is located around 900 cm^{-1}, which is due to the asymmetric stretching vibration of terminal Si—O bonds [41]; and a small shoulder at around 670 cm^{-1} indicates the stretching vibration of tetrahedral T-O groups (where T represents Si or Al) [42]. As

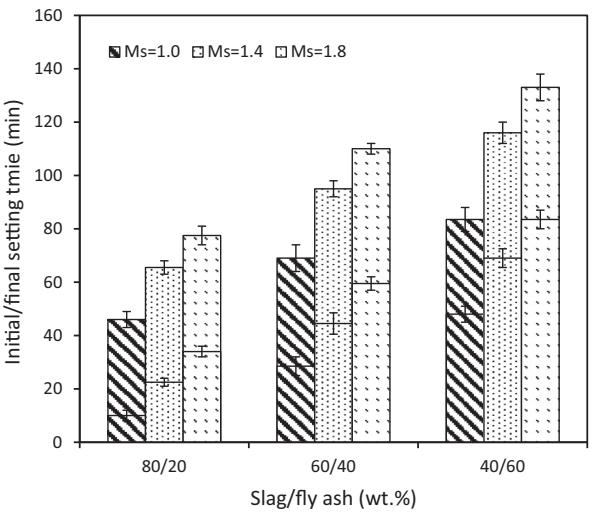

Fig. 3. Setting time of AA slag-fly ash pastes.

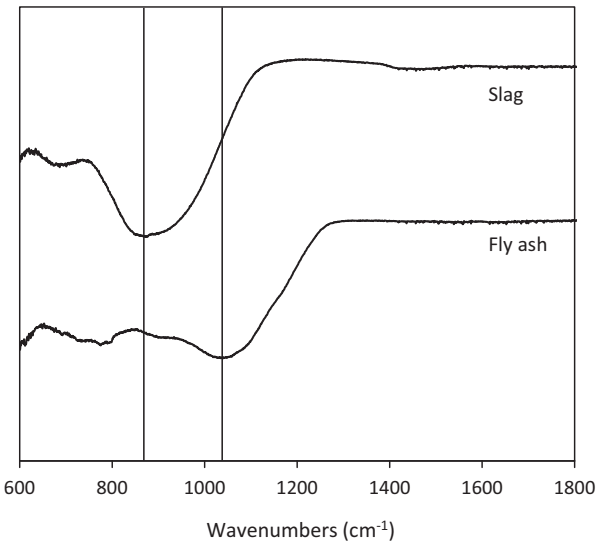

Fig. 4. FTIR spectra of the starting materials.

for the fly ash, the main absorption band is shown at around 1020 cm^{-1}, demonstrating that the structure is dominated by the bridge Si—O—T bonds [43]; while some weak absorption bands that are located around 1080, and 600–800 cm^{-1} manifest the presence of small amount of quartz and mullite [44]. The difference in the main absorption band is attributed to the structural differences of the amorphous phase within the raw materials.

Fig. 5(a) and (b) presents the infrared spectra of alkali activated slag-fly ash blends, at 1 and 28 d, respectively. Four mixtures with relatively remarkable differences in slag/fly ash ratios (8/2 and 4/6) and activator modulus (1.0 and 1.8) were chosen. Samples are labeled by the combination of slag/fly ash ratio, activator modulus and curing age, for instance "820-1" in Fig. 5(a) represents the mixes with a slag/fly ash ratio of 8/2 and activator modulus of 1.0, after 1 d of curing. After one day of activation, as can be seen from Fig. 5(a), all samples exhibit a main absorption band at similar locations that lies around 940 cm^{-1}, which is assigned to the asymmetric stretching vibration of the non-bridging Si—O bonds [41]. It indicates that the reaction product is dominated by chain structures rather than highly polymerized one; and they are generally regarded as C-A-S-H type gels with high Si and Al additions. Besides, it also shows that the gel structure of alkali activated slag-fly ash blends is relatively stable regardless of the activator parameters and raw material composition. Compared to the starting materials, the main absorption band shows an increase from 900 to 940 cm^{-1} for the slag, indicating that the Si—O networks experienced a certain degree of polymerization; while for the fly ash, the main absorption band shifts from 1020 cm^{-1} to lower numbers, implying the breakdown of the original high cross-linked bridging Si—O bonds and the polymerization process of the aluminosilicates did not take place in this blended system. All mixtures also exhibit a slight shoulder at around 875 cm^{-1}, this absorption band together with the one at 1400 cm^{-1} are assigned to the vibrations of O-C-O in carbonates [45]. Since there is no carbonate source within the raw materials, it is highly probable that a certain extent of carbonation may have occurred during the reaction or curing process. Samples with a higher slag content (80% by mass) present a more significant absorption band at around 640 cm^{-1}, which is associated with the formation vibration of TO_4 groups (where T represents Si or Al). It is more likely that this band is shifted from 670 cm^{-1} (in the unreacted slag) and indicates that structural changes have also occurred to the tetrahedral T-O groups during alkali activation. The vibration bands at 1640 cm^{-1}

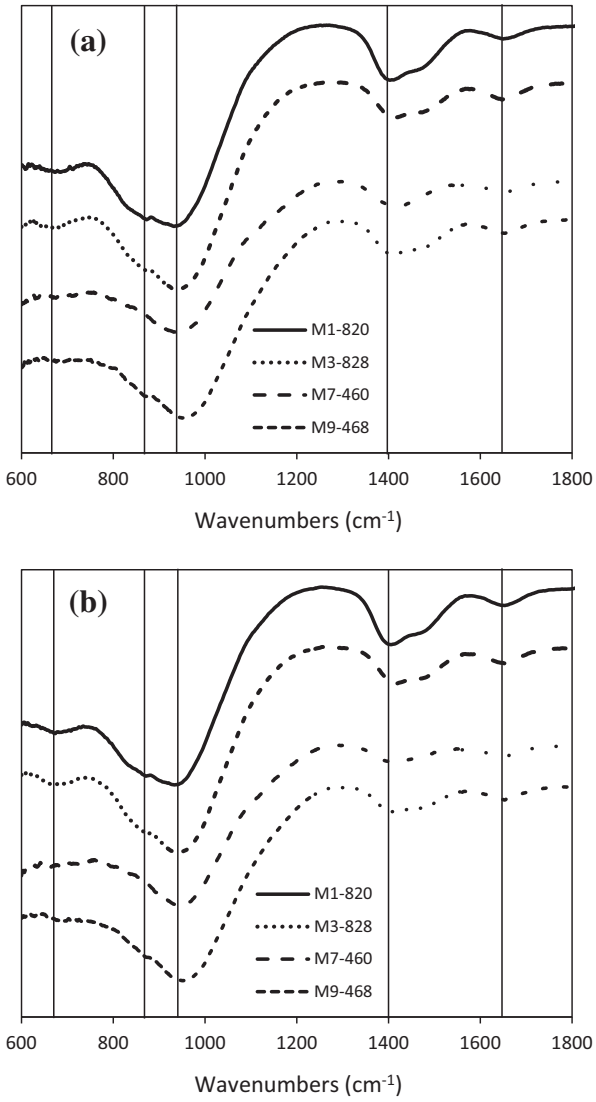

Fig. 5. FTIR spectra of AA slag-fly ash blends at 1 and 28 d (a, b).

and around 3200 cm^{-1} (not shown in the figure) in all mixes manifest the presence of bound water within the reaction products [46]. The water observed here may include both physically and chemically bound ones.

Although all samples exhibit the same type of main reaction product (chain structured C-A-S-H type gels), slight differences in the location of the main absorption peaks are still observed within a subtle scale. As can be noticed, for samples with a slag/fly ash ratio of 80/20, the location of the main absorption band is almost fixed at around 940 cm^{-1}, the changes in the applied activator modulus does not lead to a significant shift of the band location; while in mixtures with a slag/fly ash ratio of 40/60, the main absorption band slightly shifts to higher wavenumbers, implying that the reaction products in those mixes have a relatively high polymerization degree. It is more likely that the shifted band location is due to the increased fly ash content, since the activator modulus in this case also shows a negligible effect. During the reaction process, the original amorphous structure of slag and fly ash is dissolved into Ca, Si and Al units, and then those units react with each other to form C-A-S-H type gels. Thus it is possible that the higher location of the main absorption band is attributed to the increased content of Si, Al groups within the reaction products, or the insufficient dissolution of fly ash at room temperature and relative low alkali concentrations. Concerning the gel structure development, as shown in Fig. 5(a) and (b), no significant structural changes were observed between the age of 1 and 28 d, which manifestes that the main reaction process may have already finished after 1 d of curing. It should be noted that until the curing age of 28 d, samples with a slag/fly ash ratio of 40/60 still exhibit a higher wavenumber of the main absorption peak, indicating that slight but detectable gel structure differences may remain in the long term.

3.3. TG analysis

Fig. 6(a)–(d) depicts the thermogravimetric results of pastes with different slag/fly ash ratios (80/20 and 40/60) and activator moduli (1.0 and 1.8) at the age of 1, 7 and 28 d, respectively. Samples are labeled following the same rule as the ones in FTIR analysis. It is clear that a significant mass loss before around 105 °C is shown in all mixes; this is mainly attributed to the loss of physically bound water within the matrix [47]. All mixtures exhibit similar evaporable water content at the same curing age. Regardless of the manufacturing parameters and curing age, all samples present a negligible mass loss between around 105 °C and 150 °C, followed by a gradual decrease until heated to around 700 °C. The continuous mass loss after around 150 °C is generally regarded as the loss of chemically bound water due to the gradual decomposition of the reaction products (mainly C-A-S-H type gels in this case). Between around 700 °C and 1000 °C, only a very slight and moderate mass loss is shown in general. Considering no other abrupt mass losses are shown between 105 °C and 1000 °C, it can be concluded that the reaction products are mainly amorphous gels with bound water.

For samples with a slag/fly ash ratio of 40/60 and an activator modulus of 1.0, as shown in Fig. 6(a), the mass loss between around 105 °C and 1000 °C shows a small increment as a function of time, which increases from 2.9% to 3.3% between 1 and 28 d. It should be noted that the mass loss within this temperature range is not only due to the loss of chemically bound water from decomposed gels; the decomposition of the carbonates also plays a role. This is confirmed by the relatively remarkable mass loss between 600 °C and 800 °C, and the presence of carbonates observed in the FTIR results in this study. The calculated mass loss in this temperature range (600–800 °C) is approximately 1.0%, and it does not obviously change with the increase of the curing time. When increasing the activator modulus to 1.8, as shown in Fig. 6(b), the mass loss between 600 °C and 800 °C tends to be moderate. It could be an indication that samples with a lower activator modulus may exhibit a higher tendency toward carbonation. Besides, the total mass loss between 105 °C and 1000 °C is 2.3%, 3.0% and 3.0% at 1, 7 and 28 d, respectively. The slightly increased chemically bound water content after 1 d of curing suggests that the main reaction process may have already completed within the first day of curing, and the reaction at later ages present detectable but limited contribution. Previous researches on the early age reaction kinetics of silicate activated slag-fly ash blends also confirmed the completion of the main reactions during the first few hours [48,49]. Combined with the FTIR results in Section 3.2, it is reasonable to conclude that the slightly increased chemically bound water after 1 d is mainly attributed to the continuous formation of C-A-S-H type gels in a small scale, rather than generating new phases.

For a constant activator modulus, samples with higher slag contents (e.g. slag/fly ash ratio of 80/20), as presented in Fig. 6 (c) and (d), exhibit a higher mass loss between 105 °C and 1000 °C in general. For instance, the calculated chemically bound water content in Fig. 6(c) is 3.4%, 3.9% and 4.2% at 1, 7 and 28 d, respectively; which is slightly higher at each curing age compared

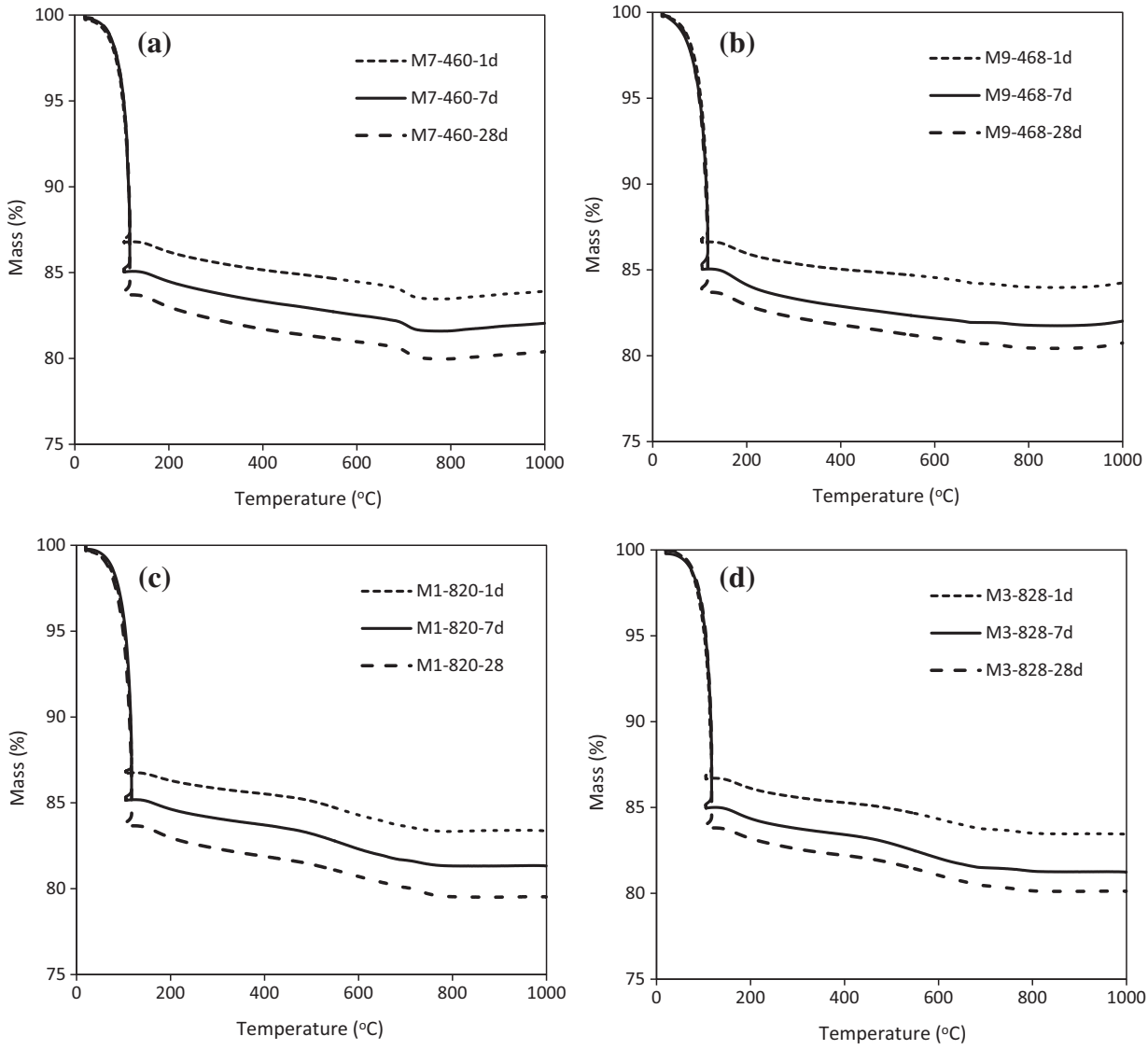

Fig. 6. TG analyses of AA slag-fly ash blends at 1, 7 and 28 d (a, b, c, d).

with the ones shown in Fig. 6(a). This phenomenon can be explained by the higher reactivity of slag than fly ash under ambient temperature due to their differences in amorphous structure, thus a higher absolute content of slag results in a higher total reaction degree with more bound water. Additionally, for a fixed slag/fly ash ratio, a slightly increased mass loss between 105 °C and 1000 °C was also observed when lowering the activator modulus, it may imply that a relatively high amount of sodium hydroxide in the activator (sodium hydroxide modified sodium silicate) exhibits a better activation effect. However, further investigation is still needed in order to understand the relations between the key manufacturing parameters and certain macro performances.

3.4. Compressive strength

The 7 and 28 d compressive strength of mortars with different activator moduli and slag/fly ash ratios are depicted in Fig. 7. Generally, the samples exhibit compressive strengths that range from 52.8 MPa to 68.4 MPa at 7 d, and 67.4 MPa to 86.4 MPa after 28 d of curing. Similar strength levels were also reported by Ng [67], in which case particle packing model was applied in the alkali activated slag-fly ash based composites. Besides, samples with higher

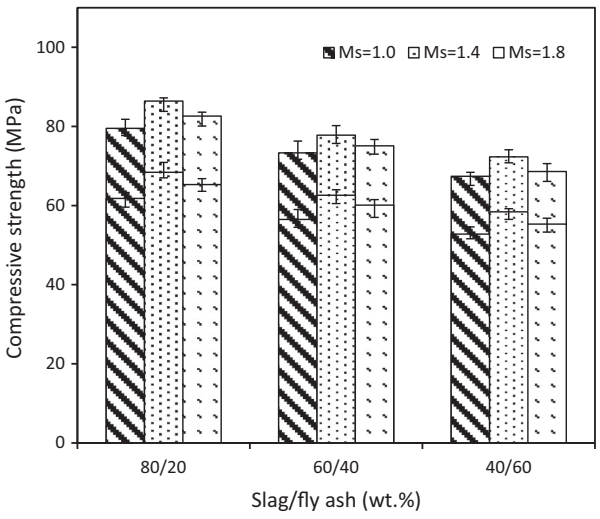

Fig. 7. 7 and 28 d compressive strength of AA slag-fly ash mortars.

slag contents show a relatively high strength and a medium activator modulus of 1.4 presents the optimum compressive strength in every case. Specifically, for mixes with a slag/fly ash ratio of 80/20, the 7 d strength is 61.8 MPa with an activator modulus of 1.0, and it increases to 68.4 MPa when increasing the activator modulus to 1.4, a further increase of the modulus to 1.8 leads to a reduction of strength to 65.3 MPa. Similar tendency is also shown at 28 d, samples with an activator modulus of 1.4 exhibits the highest strength of 86.4 MPa; while both mixes with lower or higher activator moduli show a lower compressive strength: 79.5 MPa and 82.6 MPa, respectively.

However, it seems that the strength development is not well related to the activator modulus, since the strength increasing rate between 7 and 28 d is 28.6%, 26.3% and 26.5% for samples with activator modulus of 1.0, 1.4 and 1.8, respectively. The presence of the optimal activator modulus implies that within the parameter ranges in this study, both too high or too low activator moduli may present a negative influence on strength. One possible explanation is that compared to the samples with a higher modulus, mixes with an activator modulus of 1.0 exhibit a significantly lower slump flow (see Section 3.1), and the poor workability presents a less effective dispersion of the raw materials in the fresh mix, then a slightly lower strength is consequently shown. In addition, the extra silicates that are provided by the activator also participate in the reaction process, and reaction products with different silicate contents are resulted. It indicates a critical additional silicate content, which will exhibit a relatively high strength. Besides the highest strength in each case, there is no remarkable strength difference between samples with activator moduli of 1.0 and 1.8, implying that the effect of activator modulus on strength is non-negligible but limited.

Concerning the effect of raw materials' composition, there is a gradual decrease in compressive strength when lowering the slag/fly ash ratio. As shown in Fig. 7 that for a constant activator modulus of 1.4, the 7 d compressive strength for mixes with slag/fly ash ratio of 80/20 is 68.4 MPa, which slightly decreases to 62.6 MPa and 58.4 MPa when lowering the slag content to 60% and 40%, respectively. The corresponding 28 d strength also decreases from 86.4 MPa to 77.8 MPa and 72.3 MPa, respectively. The positive effect of the slag content on compressive strength has been frequently reported in the previous studies [50–52], the beneficial effect is mainly due to its higher reactivity than fly ash under ambient temperature, and the higher content of network-modifying cations in slag leads to the formation of reaction products with more C-A-S-H type gels [53]. Then a higher strength is presented as a consequence. In addition, it can be seen that the strength variations caused by the raw materials' composition are larger than the activator modulus, indicating its relatively high dominant role in determining the mechanical properties. It should be emphasized that the mechanical property of alkali activated materials is particularly sensitive to the key manufacturing parameters such as activator type and dosage, raw materials' composition and origin, water to binder ratio and curing conditions. Thus due to the large variation of those mentioned factors, it is difficult to make effective comparison within the available literatures. However, equivalent or higher compressive strengths are achieved in general compared to other alkali activated slag-fly ash blends [61–64]. It is also clear that samples with large amounts of fly ash content in this case also exhibit excellent compressive strengths for relevant applications, for instance in samples with a slag/fly ash ratio of 40/60, the 7 d strength ranges from 52.8 MPa to 58.4 MPa while the 28 d strengths are between 67.4 MPa and 72.3 MPa. Besides, in the present study the system is investigated on the mortar level with the maximum aggregate size of 2 mm; it can be predicted that the effect of particle packing can be more prominent when larger aggregate sizes and wider particle size distributions are used. Compared to [56], by using the particle packing model, lower water binder ratios can be used for the mortar samples without a significant loss of the flowability, then higher strength are achieved based on the same materials' origin and synthesis process, indicating a higher efficiency of the utilization of the raw materials.

3.5. Porosity

The 7 and 28 d water permeable porosities of samples with slag/fly ash ratios of 80/20 and 40/60 are shown in Fig. 8. It is clear that the mixtures with a lower slag content exhibit a higher porosity, and the porosity slightly decreases with the increase of the activator modulus. For mixes with an activator modulus of 1.0, the porosity is 21.4% at 7 d for samples with a slag/fly ash ratio of 80/20, while it increases to 23.6% when shifting the slag/fly ash ratio to 40/60. Similarly, when reducing the slag content from 80% to 40%, the porosity at 7 d is increased by 10.2% and 10.0% in samples with an activator modulus of 1.4 and 1.8, respectively. However, depending on the different application levels, a balance between the setting times, slump flow, compressive strength and the costs can be achieved by the incorporation of fly ash with an appropriate amount; as can be seen that desirable strengths with other similar properties are shown in samples with high fly ash contents. It should be noted that relatively high porosities of alkali activated materials are also reported in other previous researches [57–60], this is probably due to the relatively high physically bound water content (see Fig. 6) of this type of material by nature. Between the curing age of 7 d and 28 d, a slight decrease of porosity is observed in all mixes. For samples with a slag/fly ash ratio of 40/60 and an activator modulus of 1.0, the water permeable porosity is 23.6% after 7 d of curing, and it reduces to 22.8% at 28 d. The porosity also decreased by 3.5% and 3.2% in samples with an activator modulus of 1.4 and 1.8, respectively. The slight decrease of porosity is probably attributed to the formation of reaction products at a small scale at later ages, since the slight increase in bound water is found in the thermogravimetric analysis in this study and the strength development can also be an indication. Additionally, it can be observed that there is a gradual reduction of porosity when increasing the activator modulus from 1.0 to 1.8. For instance, in samples with a slag/fly ash ratio of 80/20, the porosity at 7 d is 21.4%, 20.6% and 20.1% for mixes with activator modulus of 1.0, 1.4 and 1.8, respectively; and these values are 20.7%, 19.8% and 19.4% at the age of 28 d. It can be seen that the porosity results are not well related to the ones from compressive strength, where

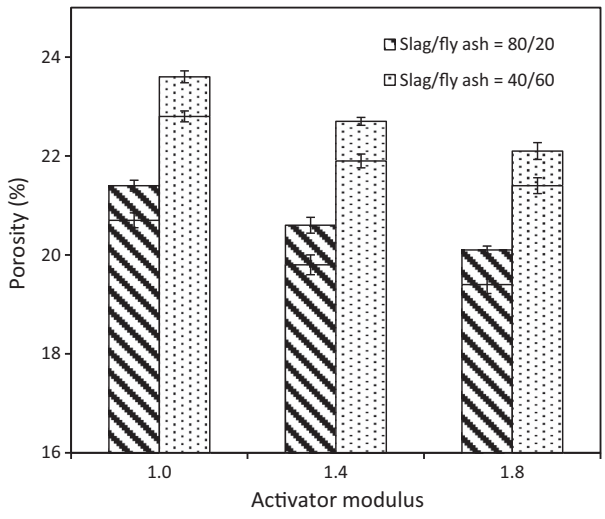

Fig. 8. 7 and 28 d porosity of AA slag-fly ash mortars.

an optimum activator modulus is shown. It demonstrates that the porosity is not the only indication of the compressive strength in this case. Since it is well known that the additional silicates that are provided by the activator participate in the reaction process and eventually become part of the reaction products, it is highly possible that the compositional difference of the reacted gels caused by the activator plays a role in determining the strength, and there may exist an optimum gel composition concerning the mechanical properties. When concerning the porosity alone, an increase of the activator modulus within a reasonable range (from 1.0 to 1.8 in this case) may always refine the pore structure due to the increased additional silicate groups.

3.6. Drying shrinkage

The drying shrinkage of samples with slag/fly ash ratios of 80/20 and 40/60 are presented in Fig. 9. It can be seen that all mixes exhibit an obvious length change over time, and the drying shrinkage is strongly affected by the raw materials' composition and the activator modulus (namely the proportions between sodium hydroxide and sodium silicate). It is commonly known that the drying shrinkage is caused by the evaporation of free water from the pores of the hardened mortar, and a higher drying shrinkage is usually shown when compared to the ordinary Portland cement. The thermogravimetry results in this study (see Fig. 6) may partly explain this phenomenon since all mixes present a relatively high proportion of physically bound water. As shown in Fig. 8, samples with a lower slag content and a lower activator modulus show a lower drying shrinkage in general. For example, with a constant slag/fly ash ratio of 80/20, the length change at the age of 28 d is around -3364×10^{-6} for mixes with an activator modulus of 1.0, while this value increases to -3996×10^{-6} and -4864×10^{-6} when increasing the activator modulus to 1.4 and 1.8, respectively. Similarly, when shifting the activator modulus from 1.0 to 1.8, the length change is increased by 29.1% and 71.3% in samples with a slag/fly ash ratio of 40/60 at 28 d. Thus it is clear that a significant increase of drying shrinkage will result when increasing the activator modulus. This is in agreement with the previous study on the drying shrinkage of alkali activated slag-fly ash blends that the higher extra silicate content from the activator is, the higher drying shrinkage is [29]. Based on the results of the porosity test in this study, it seems that the refined pore structure caused by the increased additional silicate content (increased activator modulus) may be linked to the shrinkage behaviors due to the self-desiccation. In addition, the result also implies that using activators with a lower modulus can effectively reduce the drying shrinkage to some extent.

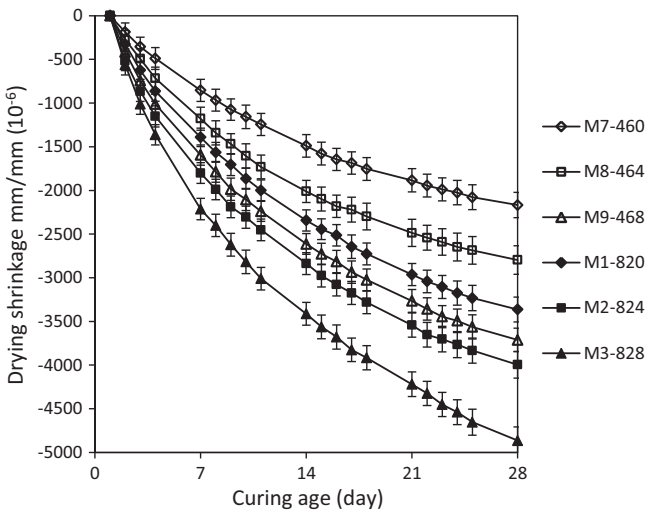

Fig. 9. Drying shrinkage of AA slag-fly ash mortars.

A significant reduction of drying shrinkage is presented when a lower slag content is used in the slag-fly ash blends. It can be seen that with a constant activator modulus, taking 1.4 as an example, the 28 d length change is -3996×10^{-6} for mixtures with a slag/fly ash ratio of 80/20; while it decreases to -2797×10^{-6} (by nearly 30.0%) when lowering the slag/fly ratio to 40/60, suggesting that replacing slag by fly ash is an ideal approach to reduce the dry shrinkage. This result is in accordance with the previous investigations that reducing the slag content in the slag-fly ash blends will lead to a decrease of drying shrinkage [54,55]. As shown in the FTIR analysis of this study, the main reaction product in the alkali activated slag-fly ash blends is a C-A-S-H type gel, which is similar to the one in alkali activated pure slag. And compared to the spectra curve of the unreacted slag, the accumulation of Si, Al groups is observed based on the fact that there is an increase in wavenumbers of the main absorption peak. While under ambient temperature, the fly ash only experienced a decomposition process without the typical polymerization between the Si, Al monomers/oligomers (as shown in Fig. 5 that there is no typical absorption bands around 1100 cm^{-1}). The reaction process of slag that is accompanied with the accumulation of silicates might be a reason of the relatively high shrinkage; while this process seems to be more moderate for fly ash. It is also possible that the typical C-A-S-H gels with low Ca/Si ratio exhibit a high tendency of shrinkage by nature, and the addition of extra Si, Al groups into the reacted gel may modify this property. In overall, both the incorporation of fly ash into slag and lowering the silicate content from activator are efficient methods of reducing the shrinkage.

4. Conclusions

This paper addresses the properties of alkali activated slag-fly ash mortars that are designed by using the modified Andreasen and Andersen packing model. Furthermore, the effects of two key manufacturing factors (slag/fly ash ratio and activator modulus) on porosity and drying shrinkage, as well as slump flow, setting times, gel structure development, and compressive strength are analyzed, and their relations are discussed. Based on the experimental results, the following conclusions can be drawn:

- A large range of slump flow (from 16.4 to 30.8 cm) and setting time (from 10/46 to 84/133 min) can be caused by both slag/fly ash ratio and activator modulus. Increasing the fly ash content in the slag-fly ash mix leads to an increased slump flow and prolonged initial/final setting time; while an increase of the activator modulus results in an increased flowability and delayed setting times. The activator modulus exhibits a more considerable effect on the fresh behaviors than the raw materials' composition.
- Gel structure development shows that the main reaction product is a C-A-S-H type gel, and it remains stable after 1 d of curing regardless of the key synthesizing factors. But samples with high fly ash contents show a slightly higher main absorption band. The chemical bond water content is around 3–4% after 28 d of curing. Mixes with higher slag contents and low activator moduli present higher bound water contents. Besides, slight gel development is still observed at later ages.
- A higher compressive strength is observed in samples with higher slag contents; and an optimum strength (from 86.4 to 72.3 MPa) is shown in mixtures with an activator modulus of 1.4 in all cases. While samples with activator moduli of 1.0 and 1.8 do not show significant differences in strength. Mixes

with higher slag contents exhibit lower porosities (around 2%) in general, and an increase of the activator modulus within the range of 1.0 and 1.8 shows a positive effect on the pore refinement. It is suggested that the porosity is not the only indication of strength; the gel composition may also play a role.

- Both raw materials' composition and activator modulus show remarkable influence on the shrinkage behavior; and the 28 d drying shrinkage can be varied from -2168×10^{-6} to -4864×10^{-6}. The incorporation of fly ash into slag can effectively reduce the shrinkage of mortar samples; also the drying shrinkage can be reduced to certain extent by decreasing the additional silicate content from the activator. Thus it is suggested that a balance between the fresh behaviors, strength, and shrinkage should be considered when determining the key manufacturing parameters of alkali activated slag-fly ash mortars.

Acknowledgements

This research was supported by China Scholarship Council and the Department of the Built Environment at Eindhoven University of Technology. The authors gratefully thank Mr. P. de Vries (ENCI B. V., the Netherlands) and Mr. J. van Eijk (Knauf Insulation, the Netherlands) for the materials supply. Furthermore, the authors wish to express their gratitude to the following sponsors of the Building Materials research group at TU Eindhoven: Rijkswaterstaat Grote Projecten en Onderhoud; Graniet-Import Benelux; Kijlstra Betonmortel; Struyk Verwo; Attero; Enci; Rijkswaterstaat Zee en Delta-District Noord; Van Gansewinkel Minerals; BTE; V.d. Bosch Beton; Selor; GMB; Geochem Research; Icopal; BN International; Eltomation; Knauf Gips; Hess AAC Systems; Kronos; Joma; CRH Europe Sustainable Concrete Centre; Cement & Beton Centrum; Heros and Inashco (in chronological order of joining).

References

[1] F. Puertas, A. Fernández-Jiménez, Mineralogical and microstructural characterisation of alkali-activated fly ash/slag pastes, Cem. Concr. Compos. 25 (2003) 287–292.
[2] P. Duxson, J.L. Provis, G.C. Lukey, J.S.J. Van Deventer, The role of inorganic polymer technology in the development of 'green concrete', Cem. Concr. Res. 37 (2007) 1590–1597.
[3] S.D. Wang, K.L. Scrivener, P.L. Pratt, Factors affecting the strength of alkali-activated slag, Cem. Concr. Res. 24 (6) (1994) 1033–1043.
[4] A. Fernández-Jiménez, I. García-Lodeiro, A. Palomo, Durable characteristics of alkali activated fly ashes, J. Mater. Sci. 42 (2007) 3055–3065.
[5] Y.Z. Hai, Venkatesh Kodur, L.Q. Shu, C. Liang, W. Bo, Development of metakaolin-fly ash based geopolymers for fire resistance applications, Constr. Build. Mater. 55 (2014) 38–45.
[6] T. Bakharev, J.G. Sanjayan, Y.B. Cheng, Resistance of alkali-activated slag concrete to acid attack, Cem. Concr. Res. 33 (2003) 1607–1611.
[7] Chao Li, Henghu Sun, Longtu Li, A review: the comparison between alkali-activated slag (Si + Ca) and metakaolin (Si + Al) cements, Cem. Concr. Res. 40 (2010) 1341–1349.
[8] A.R. Brough, A. Atkinson, Sodium silicate-based alkali-activated slag mortars: Part I. Strength, hydration and microstructure, Cem. Concr. Res. 32 (2002) 865–879.
[9] M.L. Granizo, S. Alonso, M.T. Blanco-Varela, A. Palomo, Alkaline activation of metakaolin: effect of calcium hydroxide in the products of reaction, J. Am. Ceram. Soc. 85 (1) (2002) 225–231.
[10] M. Rashad Alaa, Properties of alkali-activated fly ash concrete blended with slag, Iran. J. Mater. Sci. Eng. 10 (1) (2013) 57–64.
[11] S. Aydin, A ternary optimization of mineral additives of alkali activated cement mortars, Constr. Build. Mater. 43 (2013) 131–138.
[12] T. Sugama, L.E. Brothers, T.R. Van de Putte, Acid-resistant cements for geothermal wells: sodium silicate activated slag/fly ash blends, Adv. Cem. Res. 17 (2) (2005) 65–75.
[13] N.K. Lee, H.K. Lee, Setting and mechanical properties of alkali-activated fly ash/slag concrete manufactured at room temperature, Constr. Build. Mater. 47 (2013) 1201–1209.
[14] I. García-Lodeiro, D.E. Macphee, A. Palomo, A. Fernández-Jiménez, Effect on fresh C-S-H gels the simultaneous addition of alkali and aluminium, Cem. Concr. Res. 40 (2010) 27–32.
[15] I. Ismail, S.A. Bernal, J.L. Provis, R.S. Nicolas, S. Hamdan, J.S.J. Deventer, Modification of phase evolution in alkali-activated blast furnace slag by the incorporation of fly ash, Cem. Concr. Compos. 45 (2014) 125–135.
[16] C.K. Yip, G.C. Lukey, J.S.J. van Deventer, The coexistence of geopolymeric gel and calcium silicate hydrate at the early stage of alkaline activation, Cem. Concr. Res. 35 (2005) 1688–1697.
[17] I. García-Lodeiro, A. Fernández-Jiménez, A. Palomo, D.E. Macphee, Effect of calcium additions on N-A-S-H cementitious gels, J. Am. Ceram. Soc. (2010) 1–7.
[18] I. García-Lodeiro, A. Fernández-Jiménez, M.T. Blanco, A. Palomo, FTIR study of the sol-gel synthesis of cementitious gels: C-S-H and N-A-S-H, J. Sol-Gel Sci. Technol. 45 (2008) 63–72.
[19] I. García-Lodeiro, D.E. Macphee, A. Palomo, A. Fernández-Jiménez, Effect of alkalis on fresh C-S-H gels. FTIR analysis, Cem. Concr. Res. 39 (2009) 147–153.
[20] H.J.H. Brouwers, H.J. Radix, Self-compacting concrete: theoretical and experimental study, Cem. Concr. Res. 35 (2005) 2116–2136.
[21] G. Hüsken, H.J.H. Brouwers, Earth-moist concrete: application of a new mix design concept, Cem. Concr. Res. 38 (2008) 1246–1259.
[22] M. Hunger, A.G. Entrop, I. Mandilaras, H.J.H. Brouwers, M. Founti, The behavior of a microencapsulated phase change material in concrete, Cem. Concr. Compos. 31 (2009) 731–743.
[23] F. De Larrard, T. Sedran, Optimization of ultra-high-performance concrete by the use of a packing model, Cem. Concr. Res. 24 (1994) 997–1009.
[24] F. De Larrard, T. Sedran, Mixture-proportioning of high-performance concrete, Cem. Concr. Res. 32 (2002) 1699–1704.
[25] S.A.A.M. Fennis, J.C. Walraven, J.A. den Uijl, The use of particle packing models to design ecological concrete, Heron 54 (2009) 185–204.
[26] A.H.M. Andreasen, J. Andersen, Über die Beziehungen zwischen Kornabstufungen und Zwischenraum in Produkten aus losen Körnern (mit einigen Experimenten), Kolloid-Zeitschrift 50 (1930) 217–228 (in German).
[27] F. Collins, J. Sanjayan, Effect of pore size distribution on drying shrinking of alkali activated slag concrete, Cem. Concr. Res. 30 (2000) 1401–1406.
[28] A.A. Melo Neto, M.A. Cincotto, W. Repette, Drying and autogenous shrinkage of pastes and mortars with activated slag cement, Cem. Concr. Res. 38 (2008) 565–574.
[29] Y. Ma, G. Ye, The shrinkage of alkali activated fly ash, Cem. Concr. Res. 368 (2015) 75–82.
[30] C. Shi, Strength, pore structure and permeability of alkali-activated slag mortars, Cem. Concr. Res. 26 (1996) 1789–1799.
[31] A.M. Fernández-Jiménez, A. Palomo, C. Lopez-Hombrados, Engineering properties of alkali-activated fly ash concrete, ACI Mater. J. 103 (2006) 106–112.
[32] H.J.H. Brouwers, H.J. Radix, Self compacting concrete: theoretical and experimental study, Cem. Concr. Res. 35 (2005) 2116–2136.
[33] H.J.H. Brouwers, Particle-size distribution and packing fraction of geometric random packings, Phys. Rev. E 74 (031309) (2006) 1–14.
[34] Q.L. Yu, P. Spiesz, H.J.H. Brouwers, Ultra-lightweight concrete: conceptual design and performance evaluation, Cem. Concr. Compos. 61 (2015) 18–28.
[35] R. Yu, P. Spiesz, H.J.H. Brouwers, Mix design and properties assessment of Ultra-High Performance Fibre Reinforced Concrete (UHPFRC), Cem. Concr. Res. 56 (2014) 29–39.
[36] G. Hüsken, H.J.H. Brouwers, A new mix design concept for earth-moist concrete: a theoretical and experimental study, Cem. Concr. Res. 38 (2008) 1246–1259.
[37] British standard EN 1015–3,, Methods of Test for Mortar for Masonry Part 3: Determination of Consistence of Fresh Mortar, 1999.
[38] British standard EN 196-3, Methods of Testing Cement Part 3: Determination of Setting Times and Soundness, 2005.
[39] British standard EN 196-1, Methods of Testing Cement Part 1: Determination of Strength, 2005.
[40] NT Build 492, Concrete, Mortar and Cement-based Repair Materials: Chloride Migration Coefficient from Non-steady-state Migration Experiments, 1999.
[41] Z.H. Zhang, H. Wang, J.L. Provis, F. Bullen, A. Reid, Y.C. Zhu, Quantitative kinetic and structural analysis of geopolymers. Part 1. The activation of metakaolin with sodium hydroxide, Therm. Acta 539 (2012) 23–33.
[42] G. Kovalchuk, A. Fernandez-Jimenez, A. Palomo, Alkali-activated fly ash: effect of thermal curing conditions on mechanical and microstructural development – Part II, Fuel 86 (2007) 315–322.
[43] A. Hajimohammadi, J.L. Provis, J.S.J. Deventer, Time-resolved and spatially resolved infrared spectroscopic observation of seeded nucleation controlling geopolymer gel formation, J. Colloid Interface Sci. 357 (2011) 384–392.
[44] M. Criado, A. Fernandez-Jimenez, A. Palomo, Alkali activation of fly ash: effect of the SiO_2/Na_2O ratio Part I: FTIR study, Microporous Mesoporous Mater. 106 (2007) 180–191.
[45] S.A. Bernal, J.L. Provis, V. Rose, A. Mejía de Gutierrez, Evolution of binder structure in sodium silicate-activated slag-metakaolin blends, Cem. Concr. Compos. 33 (2011) 46–54.
[46] P. Yu, R.J. Kirkpatrick, B. Poe, P.F. McMillan, X. Cong, Structure of calcium silicate hydrate (C-S-H): near-, mid-, and far-infrared spectroscopy, J. Am. Ceram. Soc. 82 (3) (1999) 742–748.
[47] D.L.Y. Kong, J.G. Sanjayan, Effect of elevated temperatures on geopolymer paste, mortar and concrete, Cem. Concr. Res. 40 (2010) 334–339.
[48] X. Gao, Q.L. Yu, H.J.H. Brouwers, Reaction kinetics, gel character and strength of ambient temperature cured alkali activated slag-fly ash blends, Constr. Build. Mater. 80 (2015) 105–115.
[49] S. Chithiraputhiran, N. Neithalath, Isothermal reaction kinetics and temperature dependence of alkali activation of slag, fly ash and their blends, Constr. Build. Mater. 45 (2013) 233–242.

[50] S. Kumar, R. Kumar, S.P. Mehrotra, Influence of granulated blast furnace slag on the reaction, structure and properties of fly ash based geopolymer, J. Mater. Sci. 45 (3) (2010) 607–615.
[51] J.I. Escalante García, K. Campos-Venegas, A. Gorokhovsky, A. Fernández, Cementitious composites of pulverised fuel ash and blast furnace slag activated by sodium silicate: effect of Na_2O concentration and modulus, Adv. Appl. Ceram. 105 (4) (2006) 201–208.
[52] W.G. Shen, Y.H. Wang, T. Zhang, M.K. Zhou, J.S. Li, X.Y. Cui, Magnesia modification of alkali-activated slag fly ash cement, J. Wuhan Univ. Technol. Mater. Sci. Ed. 26 (2011) 121–125.
[53] J.E. Oh, Y.B. Jun, Y. Jeong, J.M. Paulo, The importance of the network-modifying element content in fly ash as a simple measure to predict its strength potential for alkali-activation, Cem. Concr. Compos. 57 (2015) 44–54.
[54] M. Chi, R. Huang, Binding mechanism and properties of alkali-activated fly ash/slag mortars, Constr. Build. Mater. 40 (2013) 291–298.
[55] N.K. Lee, J.G. Jang, H.K. Lee, Shrinkage characteristics of alkali-activated fly ash/slag paste and mortar at early ages, Cem. Concr. Compos. 53 (2014) 239–248.
[56] X. Gao, Q.L. Yu, H.J.H. Brouwers, Properties of alkali activated slag-fly ash blends with limestone addition, Cem. Concr. Compos. 59 (2015) 119–128.
[57] Y.W. Ma, Microstructure and Engineering Properties of Alkali Activated Fly Ash (PhD thesis), Delft University of Technology, Delft, The Netherlands, 2013.
[58] J.L. Provis, R.J. Myers, C.E. White, V. Rose, J.S.J. Deventer, X-ray microtomography shows pore structure and tortuosity in alkali-activated binders, Cem. Concr. Res. 42 (2012) 855–864.
[59] I. Balczár, T. Korim, A. Dobrádi, Correlation of strength to apparent porosity of geopolymers – understanding through variations of setting time, Constr. Build. Mater. 93 (2015) 983–988.
[60] M.S. Ko, H.Y. Chen, S.J. Lyu, T.T. Wang, T.H. Ueng, Permeation characteristics and impact factors of geopolymers made of kaolin, Constr. Build. Mater. 93 (2015) 301–308.
[61] M. Rashad Alaa, A comprehensive overview about the influence of different additives on the properties of alkali-activated slag – a guide for Civil Engineer, Constr. Build. Mater. 47 (2013) 29–55.
[62] A. Islam, U.J. Alengaram, M.Z. Jumaat, I.I. Bashar, The development of compressive strength of ground granulated blast furnace slag-palm oil fuel ash-fly ash based geopolymer mortar, Mater. Des. 56 (2014) 833–841.
[63] S. Aydın, A Ternary Optimisation of Mineral Additives of Alkali Activated Cement Mortars, Constr. Build. Mater. 43 (2013) 131–138.
[64] F. Puertas, S. MartõÂnez-RamõÂrez, S. Alonso, T. VaÂzquez, Alkali-activated fly ash/slag cement Strength behaviour and hydration products, Cem. Concr. Res. 30 (2000) 1625–1632.
[65] Q.L. Yu, H.J.H. Brouwers, Development of a self-compacting gypsum-based lightweight composite, Cem. Concr. Compos. 34 (2012) 1033–1043.
[66] Q.L. Yu, H.J.H. Brouwers, Microstructure and mechanical properties of β-hemihydrate produced gypsum: an insight from its hydration process, Constr. Build. Mater. 25 (2011) 3149–3157.
[67] T.S. Ng, S.J. Foster, Development of a mix design methodology for high-performance geopolymer mortars, Struct. Concr. 14 (2) (2013) 148–156.
[68] P.H.R. Borges, L.F. Fonseca, V.A. Nunes, T.H. Panzera, C.C. Martuscelli, Andreasen particle packing method on the development of geopolymer concrete for civil engineering, J. Mater. Civ. Eng. 26 (4) (2014) 692–697.
[69] N.K. Lee, H.K. Lee, Reactivity and reaction products of alkali-activated, fly ash-slag paste, Constr. Build. Mater. 81 (2015) 303–312.